 doi:10.20944/preprints201808.0354.v1

# Significant enhancement of hydrogen-sensing properties of ZnO nanofibers through NiO loading

**Jae-Hyoung Lee[1], Jin-Young Kim[1], Ali Mirzaei[2,3], Hyoun Woo Kim[2,4,*], Sang Sub Kim[1,**]**

[1]*Department of Materials Science and Engineering, Inha University, Incheon 402-751, Republic of Korea*

[2]*The Research Institute of Industrial Science, Hanyang University, Seoul 133-791, Republic of Korea*

[3]*Department of Materials Science and Engineering, Shiraz University of Technology, Shiraz, Iran*

[4]*Division of Materials Science and Engineering, Hanyang University, Seoul 133-791, Republic of Korea*

*Corresponding author: hyounwoo@hanyang.ac.kr

**Corresponding author: sangsubkim@inha.ac.kr

**Abstract**

Metal oxide p-n heterojunction nanofibers (NFs) are among the most promising approaches to enhancing the efficiency of gas sensors. In this paper, we report the preparation of a series of p-NiO-loaded n-ZnO NFs, namely (1-x) ZnO-xNiO (x=0.03, 0.05, and 0.1 wt%), for hydrogen gas sensing experiments. Samples were prepared through the electrospinning technique followed by a calcination process. The sensing experiments showed that the sample with 0.05 wt% NiO loading resulted in the highest sensing performance at an optimal sensing temperature of 200 °C. The sensing mechanism is discussed in detail and contributions of the p-n heterojunctions, metallization of ZnO and catalytic effect of NiO on the sensing enhancements of an optimized gas sensor are analyzed. This study demonstrates the possibility of fabricating high-performance $H_2$ sensors through the optimization of p-type metal oxide loading on the surfaces of n-type metal oxides.

**Key words:** ZnO; NiO loading; p-n heterojunction; Nanofiber; Gas sensor; Sensing mechanism

 doi:10.20944/preprints201808.0354.v1

## 1. Introduction

Among various available gas sensors, metal oxides are one of the most promising gas sensors for sensing hydrogen gas [1]. This stems from their advantages in terms of high sensitivity and stability, low fabrication costs, and simplicity of use [2]. In particular, gas sensors fabricated from one-dimensional (1D) nanostructured metal oxides have become very popular in recent years based on their small size and large surface area, which results in numerous adsorption sites for target gases and facilitates rapid diffusion of gas molecules [3]. Furthermore, 1D nanostructures can be easily synthesized at low cost through simple procedures [4]. Therefore, many researchers have studied the gas sensing characteristics of 1D nanostructured metal oxides [5,6].

Among the different 1D nanostructures utilized for sensing purposes, metal oxides with nanofiber (NF) morphologies are very popular. In addition to their high surface area, they contain ultrafine nanograins, which further increase the number adsorption sites for target gases [7-9]. Another advantage of NFs is their simple and inexpensive synthesis through the electrospinning technique [10]. Accordingly, there have been many studies on gas sensors prepared through the electrospinning technique [11,12].

ZnO NFs are one of the most promising n-type oxides for gas sensing, based on their large band gap, high chemical and thermal stability, low price, high mobility of charge carriers, and the intrinsic sensitivity of ZnO [13,14]. They also benefit from high surface area based on their NF morphology [15]. For hydrogen sensing in particular, the metallization effect of ZnO (where the outer surfaces of ZnO are reduced to metallic zinc with high conductivity) in an $H_2$ atmosphere can significantly affect the sensing properties of gas sensors [16]. However, for increasingly strict accuracy standards, ZnO-based gas sensors with better performance are required. One popular method to increase the sensitivity of ZnO NF gas sensors is to create n-p heterojunction NFs by adding a p-type metal oxide to an n-type ZnO. For p-n heterojunctions, based on the transfer of electrons from n-ZnO to a p-type metal oxide, the resistance of the gas sensor is high in air. Upon exposing such a sensor to hydrogen gas, a large change in sensor resistance will lead to a stronger response compared to a pure ZnO NF sensor. Furthermore, through the injection of $H_2$ gas, metallization of ZnO surfaces can occur, resulting in a semi-conductor-to-metallic

Preprints (www.preprints.org) | NOT PEER-REVIEWED | Posted: 20 August 2018 doi:10.20944/preprints201808.0354.v1

conversion. Therefore, the heterojunctions between n-ZnO and p-type metal oxides are destroyed, which changes the resistance of a gas sensor [16] [17]. Accordingly, sensors fabricated from ZnO NFs loaded with a p-type metal oxide are expected to show excellent hydrogen sensing performance.

Among available p-type metal oxides, NiO is particularly important for sensing purposes based on its excellent structural stability, high tendency toward the adsorption of oxygen, and strong catalytic activity. Therefore, it has been extensively investigated for sensing of different gases [18,19]. Through the combination of n-ZnO and p-NiO, it is possible to develop gas sensors with superior sensing performance. For example, Liu et al. [20] demonstrated the superior acetone sensing performance of ZnO-NiO nanocomposites compared to pure ZnO. Deng et al. [18] reported the superior ethanol sensing properties of ZnO-NiO composites compared to pure NiO sensors.

However, most researchers have simply studied the gas sensing properties of one particular composition without performing any compositional optimization. Because the final gas response strongly depends on the composition of a gas sensor, it is necessary to explore the gas sensing properties of a series of compositions. To address this issue, in this study, we prepared three NiO-loaded ZnO NF gas sensors with different amounts of NiO (0.03, 0.05, and 0.1 wt%) to study the effects of composition on the hydrogen sensing behavior of the resultant gas sensors. Hdrogen gas sensing experiments revealed that the sensor with 0.05 wt% NiO loading had the strongest gas response. The strong response of the optimized NiO-loaded ZnO NF gas sensor was mainly caused by the metallization effect of ZnO and formation of n-ZnO/p-NiO heterojunctions. This study demonstrates the need for compositional optimization to achieve the strongest possible gas response in p-type-loaded n-type metal oxides.

## 2. Materials and Methods

### 2.1. Preparation of the solution for electrospinning

Analytical grades of polyvinyl alcohol (PVA, Mw = 80,000), zinc chloride dihydrate ($ZnCl_2 \cdot 2H_2O$), and nickel (II) acetate tetrahydrate ($Ni(CH_3COO)_2 \cdot 4H_2O$) were provided by Sigma-Aldrich. Deionized (DI) water was utilized as a solvent for the preparation of all solutions. First, PVA was added to DI water and stirred at 70 °C for 4 h to create a 10-wt% PVA aqueous solution. Subsequently, $ZnCl_2 \cdot 2H_2O$ and $Ni(CH_3COO)_2 \cdot 4H_2O$ solutions were added to

Preprints (www.preprints.org) | NOT PEER-REVIEWED | Posted: 20 August 2018 doi:10.20944/preprints201808.0354.v1

the polymer solution and stirred for 12 h. The final viscous solutions for electrospinning were then prepared. The amount of $Ni^{+2}$ precursor was changed to prepare solutions with different nominal compositions of NiO (0.03, 0.05, and 0.1 wt%) for the final samples.

### 2.2. Electrospinning

The electrospinning solution was loaded into a plastic syringe with a metallic needle. To initiate and accelerate electrospinning, a large positive voltage (+15 kV) and large negative voltage (–10 kV) were applied to the needle and Al collector, respectively. During electrospinning, the distance between the tip of the needle and collector was fixed as 0.2 m and the feed rate was set to 0.01 ml/h. The as-synthesized NFs were annealed at 600 °C for 2 h to remove the polymer and water to obtain crystalline phases.

### 2.3. Material characterization

The morphological features of the synthesized products were studied through field-emission scanning electron microscopy (FE-SEM, Hitachi-S-4200). Additional details of microstructural features were studied through transmission electron microscopy (TEM) with a JEOL JEM-3010. Elemental analysis was performed utilizing an energy-dispersive X-ray spectrometer (EDS) incorporated in the TEM.

### 2.4. Gas sensing measurements

The sensing experiments in this study were similar to those described in our previous paper [21]. To fabricate gas sensors, Ti (~50-nm thickness) and Pt (~200-nm thickness) electrodes were sequentially sputter-deposited onto the synthesized NFs that had been deposited on the $SiO_2$-grown Si substrates (200-nm thickness). Sensing tests were performed utilizing a gas dilution and testing system. The gas concentrations were precisely controlled by varying the mixture ratio of the target gas and dry air by utilizing mass flow controllers. The sensing properties of the gas sensors were investigated in the presence of $H_2$ gas as the main target gas and the selectivity of the optimized sensor was tested in the presence of CO and $C_6H_6$ gases at the optimized temperature of 200 °C. The resistances of the gas sensors in air ($R_0$) and in the presence of the target gas ($R_g$) were recorded utilizing a Keithley source meter. Sensor`s sensitivity was calculated as $R = (R_0-R_g)/R_0=\Delta R/R_0$. Response and recovery times were defined as the time required for the change in the resistance to reach 90% of the final value after the injection and

Preprints (www.preprints.org) | NOT PEER-REVIEWED | Posted: 20 August 2018 doi:10.20944/preprints201808.0354.v1

stoppage of $H_2$ gas, respectively. Figure 1 shows an illustration of the synthesis steps and preparation of the gas sensors.

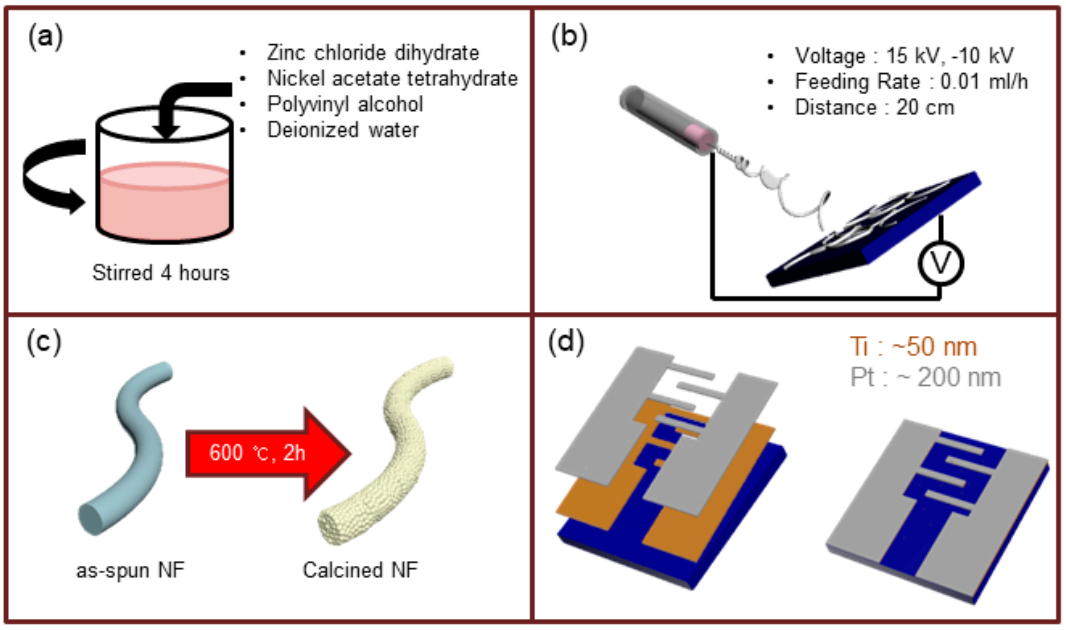


**Figure. 1.** Schematic illustration of preparation steps for the synthesis of NiO-loaded ZnO NFs: (a) preparation of viscous solution for electrospinning, (b) electrospinning procedure, (c) calcination of synthesized NFs, and (d) sensor fabrication.

## 3. Results and Discussion

### 3.1 Morphological and structural analyses

Figure 2a presents FE-SEM images of the as-spun NFs prior to calcination. They had a smooth morphology similar to nanowires (NWs) and without any nanograins. However, after calcination as a result of the evaporation of the solvent and polymer, the surfaces became rough. Figure 2 b-d present FE-SEM images of 0.97ZnO-0.03NiO, 0.95ZnO-0.05NiO and 0.90ZnO-0.1NiO NFs, respectively. They clearly reveal formation of NFs with lengths up to several micrometers. The insets in these figures show ultrafine grains on the surfaces of the synthesized NFs. This is a unique feature of NFs that discriminates NFs from NWs. These nanograins play the role of double Schottky barriers to electron transfer, which enhance the gas sensing performance of the

Preprints (www.preprints.org) | NOT PEER-REVIEWED | Posted: 20 August 2018 doi:10.20944/preprints201808.0354.v1

sensors. The diameters of the NFs is in the range of 125–150 nm. The fabricated NFs have a consistent diameter because the calcination temperature was the same for all samples and the amount of loaded NiO was not significantly different between the samples.

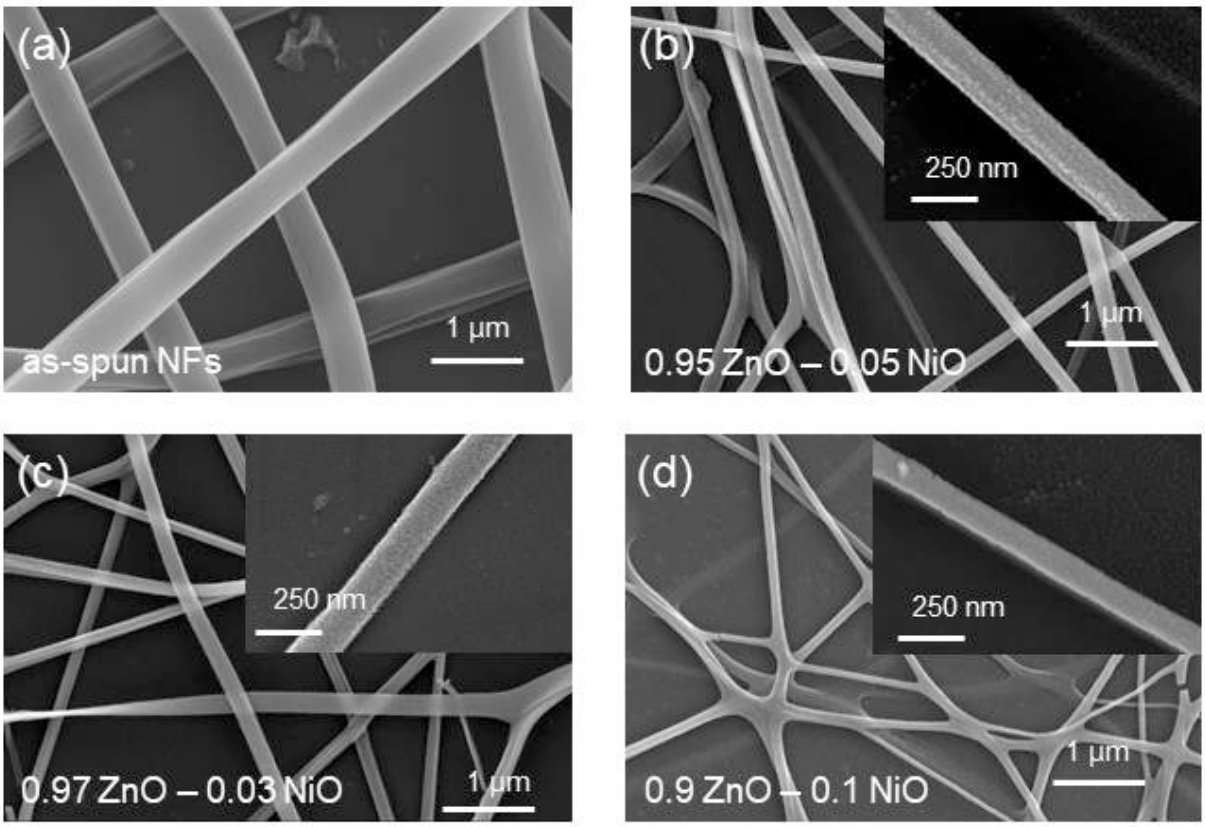


**Figure. 2.** FE-SEM images: (a) 0.03 wt% NiO-loaded ZnO NFs before calcination, (b) 0.03 wt% NiO-loaded ZnO NFs after calcination, (c) 0.05 wt% NiO-loaded ZnO NFs after calcination, and (d) 0.1 wt% NiO-loaded ZnO NFs after calcination. Insets show corresponding magnified FE-SEM images.

Figure 3a presents a typical TEM micrograph of ZnO-NiO NFs with diameters of approximately 200 nm. Figure 3b presents a lattice-resolved TEM micrograph. Interplanar distances of 0.25 nm and 0.24 nm can be indexed to the (101) and (111) planes of ZnO and NiO, respectively, demonstrating the coexistence of crystalline ZnO and NiO crystals in the synthesized NFs. Figure 3c–e present EDS color-mapping analyses of 0.95ZnO-0.05NiO NFs, confirming the coexistence of Zn, Ni, and O elements.

Preprints (www.preprints.org) | NOT PEER-REVIEWED | Posted: 20 August 2018 doi:10.20944/preprints201808.0354.v1

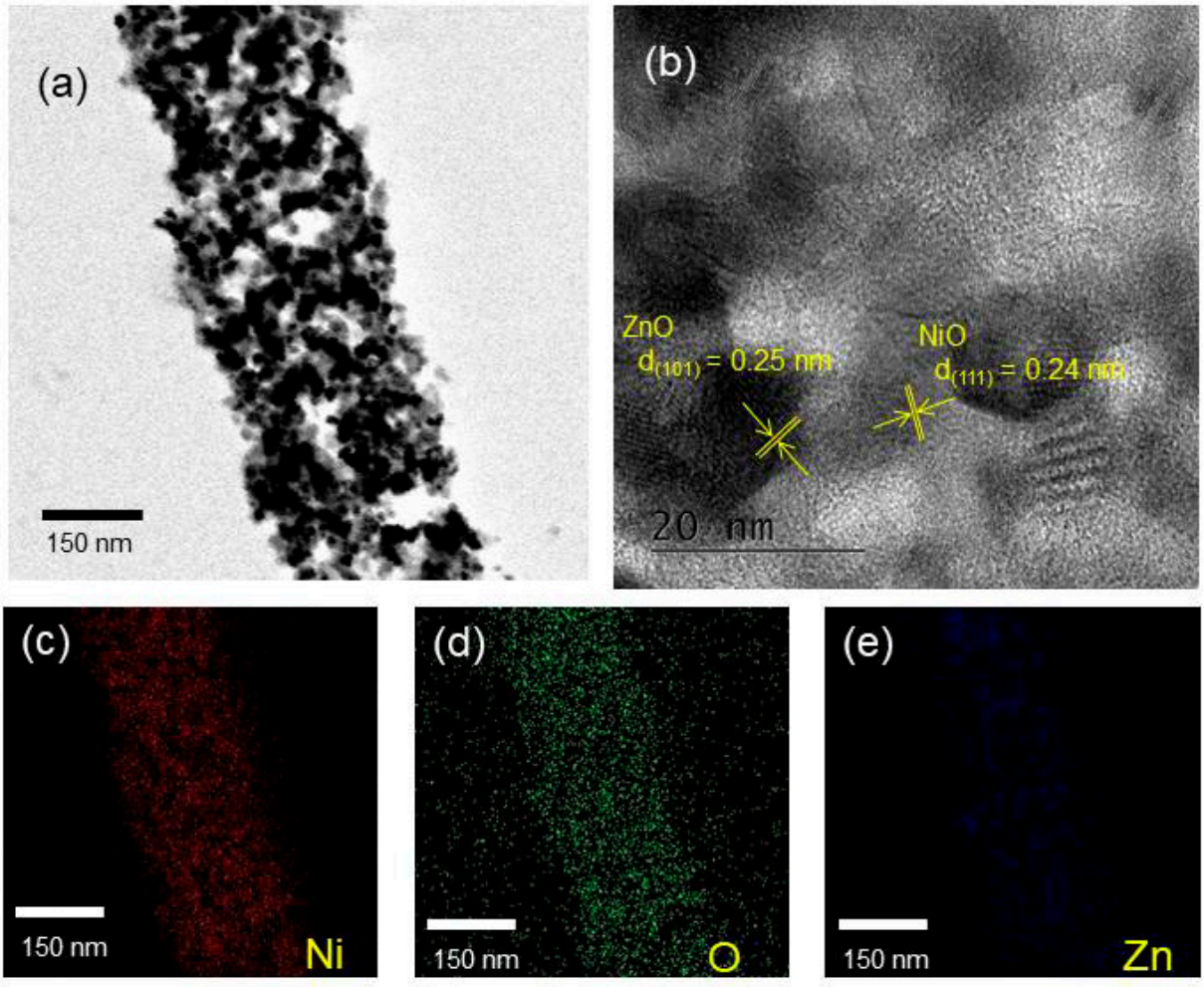


**Figure. 3.** (a) Typical high-magnification TEM image of ZnO-NiO composite NFs, (b) corresponding lattice-resolved TEM image showing the lattice fringes of ZnO and NiO, and (c)-(e) EDS color-mapping analyses of 0.05 wt% NiO-loaded ZnO NFs.

### 3.2 Gas sensing properties

Hydrogen is a promising energy source based on several advantages, including renewability, abundance, efficiency, and environmental friendliness. However, it is highly explosive in concentrations above 4 vol% in air. Therefore, the fabrication of high-quality gas sensors for $H_2$ sensing is urgent [22,23]. Accordingly, our sensor with the 0.97ZnO-0.03NiO composition was exposed to 1-, 5-, and 10-ppm $H_2$ gas at various temperatures (50–300 °C) in 50 °C steps to find the optimal working temperature. Figure 4 presents the normalized dynamic resistance of the

Preprints (www.preprints.org) | NOT PEER-REVIEWED | Posted: 20 August 2018 doi:10.20944/preprints201808.0354.v1

0.97ZnO-0.03NiO sensor at different sensing temperatures.

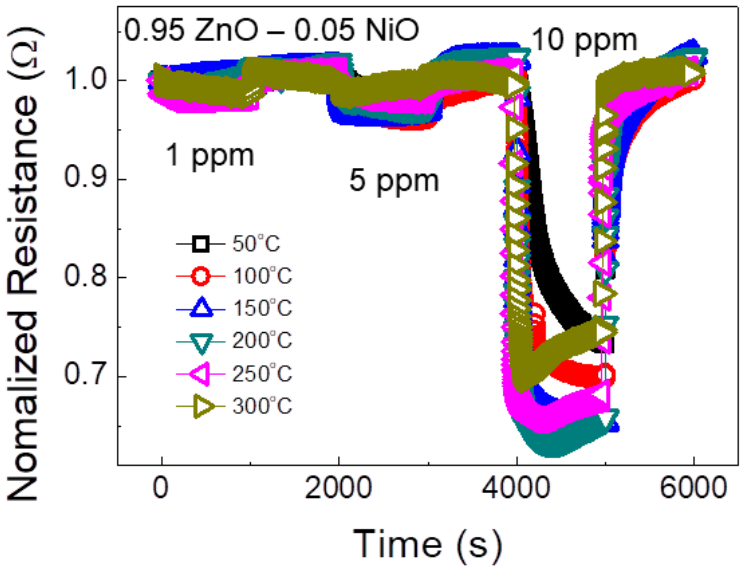


**Figure. 4.** Dynamic normalized resistance curves of 0.05 wt% NiO-loaded ZnO NF sensor for 1-, 5-, and 10-ppm $H_2$ gas at different sensing temperatures.

As it can be seen, upon exposure to $H_2$ gas at all temperatures, the resistance decreases. Upon the stoppage of $H_2$ and introduction of air, the resistance returns to its original value. Because $H_2$ gas is a reducing gas, this behavior demonstrates the n-type nature of sensor, resulting from the n-type semiconducting nature of ZnO, which is the major constituent of the proposed NiO-loaded ZnO NF gas sensor. Furthermore, the reversibility of the sensor is excellent, meaning its signal returns to the air value after the reintroduction of air. Figure 5 plots the responses of the 0.97ZnO-0.03NiO sensor to 10-ppm $H_2$ gas versus sensing temperature. This plot shows a peak at 200 °C, where the maximum response was observed for 10-ppm $H_2$ gas. At lower temperatures, the activation energy for the adsorption of $H_2$ is insufficient. At higher temperatures, the rate of gas desorption is much higher than the adsorption rate, meaning the gas escapes prior to effective adsorption on the surface of sensor [24].

Preprints (www.preprints.org) | NOT PEER-REVIEWED | Posted: 20 August 2018 doi:10.20944/preprints201808.0354.v1

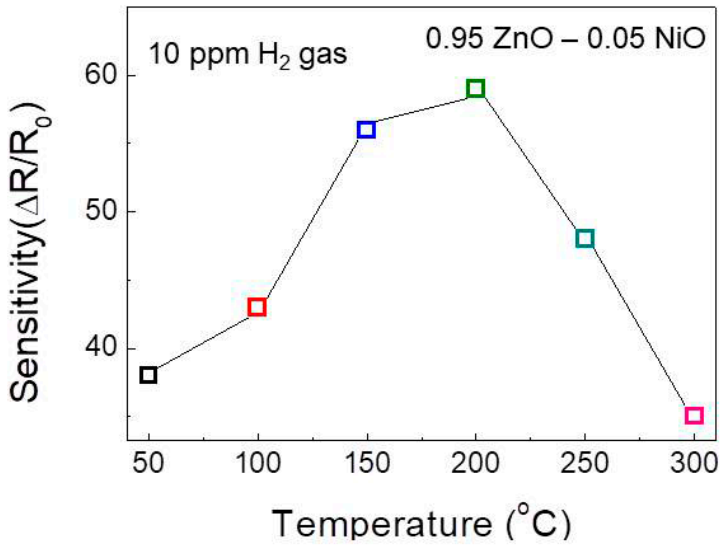


**Figure. 5.** Dependence of $H_2$ gas response on sensing temperature for 0.05 wt% NiO-loaded ZnO NF sensor.

The response and recovery times of the gas sensor at different temperatures in the presence of 10-ppm $H_2$ are presented in Figure 6a. The gas sensor shows relatively fast dynamic times because of its 1D nanostructure. This morphology facilitates rapid mass transfer of $H_2$ molecules to and from the inner regions of the sensor and improves the speed at which charge carriers can traverse the barriers along the NFs [25]. When increasing the sensing temperature, both the response and recovery times decrease because of faster gas diffusion. Figure 6b shows the decrease in the initial resistance of the sensor with increasing sensing temperature. This behavior is caused by the fact that with an increase in temperature, more electrons in the valence band of ZnO exit to the conduction band, meaning the conductivity increases. To find the optimal composition for NF sensors, 0.03, 0.05, and 0.1 wt% NiO-loaded ZnO NF sensors were exposed to 1-, 5-, and 10-ppm $H_2$ gas at 200 °C, which was identified as the optimal temperature.

Preprints (www.preprints.org) | NOT PEER-REVIEWED | Posted: 20 August 2018 doi:10.20944/preprints201808.0354.v1

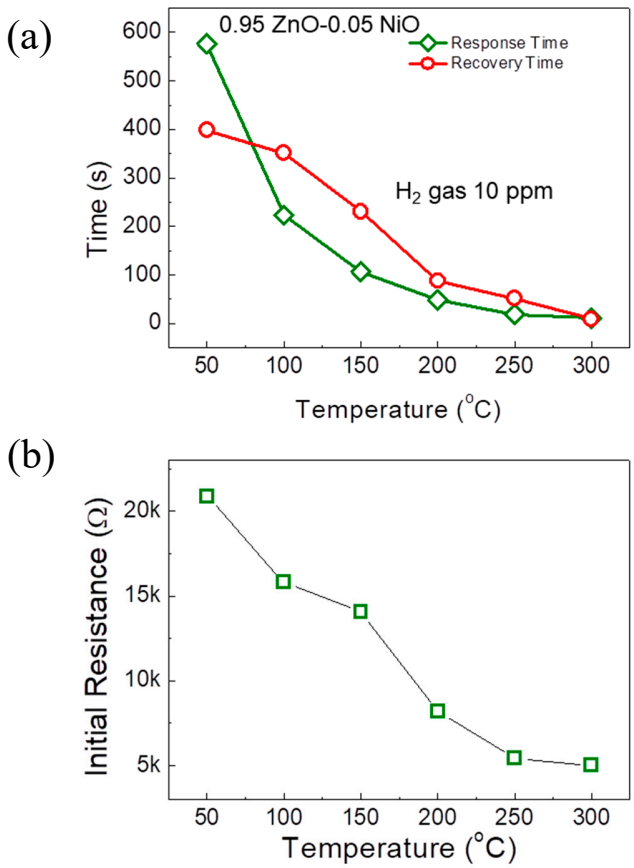


**Figure. 6.** (a) Response and recovery times of 0.05 wt% NiO-loaded ZnO NF sensor and (b) initial resistance of 0.05 wt% NiO-loaded ZnO NF sensor as a function of sensing temperature.

Figure 7a presents dynamic normalized resistance plots of the sensors when they were exposed to $H_2$ gas. The sensors did not show a meaningful response to 1-ppm $H_2$ gas, but responses to 5- and 10-ppm $H_2$ gas are clearly visible. Figure 7b illustrates the dependency of the responses on the composition of the sensors. With an increase in NiO loading from x=0.03 to 0.05 wt%, the sensing performance increased. With a further increase in the amount of NiO to 0.1 wt%, the sensitivity decreases.

Preprints (www.preprints.org) | NOT PEER-REVIEWED | Posted: 20 August 2018 doi:10.20944/preprints201808.0354.v1

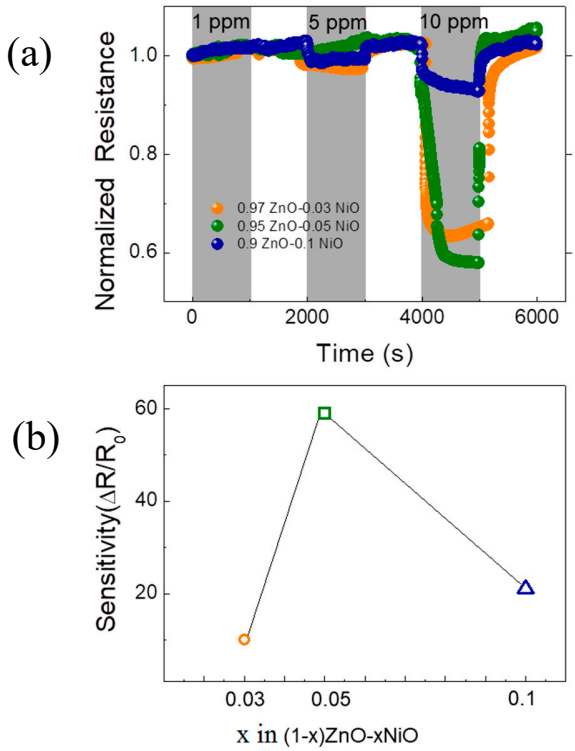


**Figure. 7.** (a) Dynamic normalized resistance curves of different sensors for various concentrations of $H_2$ gas at optimal sensing temperature of 200 °C and (b) corresponding responses for different sensor compositions.

The selectivity of the optimized sensor (0.05 wt% NiO-loaded ZnO) was analyzed by exposing the sensor to CO and $C_6H_6$ gases. Figure 8a presents the dynamic resistance curves of the gas sensor towards CO and $C_6H_6$ gases, as well as the curve for $H_2$ gas. As shown in the selectivity pattern presented in Figure 8b, the sensor demonstrates the highest response to $H_2$ gas, followed by the $C_6H_6$ and CO gases.

Preprints (www.preprints.org) | NOT PEER-REVIEWED | Posted: 20 August 2018 doi:10.20944/preprints201808.0354.v1

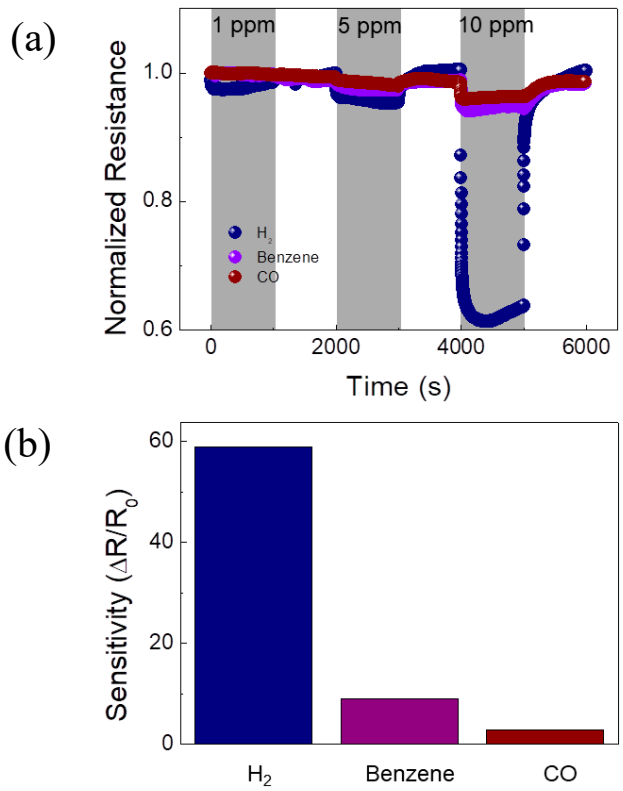


**Figure. 8.** (a). Dynamic normalized resistance curves of 0.05 wt% NiO-loaded ZnO NF gas sensor for 1-, 5-, and 10-ppm concentrations of $H_2$, CO, and $C_6H_6$ gases at 200 °C. (b) Corresponding selectivity histogram.

### 3.3 Gas sensing mechanism

When a metal-oxide-based gas sensor is exposed to a target gas, its resistance changes. By measuring this change, the nature and concentration of the target gas can be determined. First, when the NiO-loaded ZnO NF sensor is in an air environment, the oxygen gas in air is adsorbed on the surface of the sensor [26,27]:

$$O_2(g) \rightarrow O_2(ads) \quad (1)$$

$$O_2(ads) + e^- \rightarrow O_2^-(ads) \quad (2)$$

$$O_2^- + e^- \rightarrow 2O^- \quad (3)$$

Preprints (www.preprints.org) | NOT PEER-REVIEWED | Posted: 20 August 2018 doi:10.20944/preprints201808.0354.v1

$$O^- + e^- \rightarrow O^{2-} \quad (4)$$

$O^{2-}_{(ads)}$ is typically introduced at high temperatures, whereas the other oxygen species are stable at lower temperatures [28]. In general, $O_2^-$, $O^-$, and $O^{2-}$ are stable at <150 °C, 150–400 °C, and > 400 °C, respectively [29]. Therefore, at a sensing temperature of 200 °C, the dominant oxygen species can be assumed to be $O^-$.

According to above reactions, the oxygen species can extract electrons from the conduction band of ZnO, which results in the creation of an electron-depletion layer on the outer surfaces of ZnO in air. Additionally, in NiO-loaded ZnO NFs, there are two different types of semiconducting materials in which the majority of carriers are electrons (in ZnO) and holes (in NiO). When they are in direct contact, the electrons in ZnO flow into NiO to equate their Fermi levels (Figure 9a). Accordingly, the width of the depletion layer in ZnO NFs increases compared to pure ZnO and results in a higher resistance for the NiO-loaded sensor compared to pure ZnO. Therefore, it can be concluded that in ZnO-NiO composite NFs, there are two types of depletion layers: one is created by the abstraction of electrons by oxygen gas in the air and another is created by the formation of p-NiO/n-ZnO heterojunctions. When the sensor is in an $H_2$ atmosphere, hydrogen molecules react with adsorbed oxygen ions on the surface of the gas sensor (Figure 9b) according to the following equation [30]:

$$H_2 + O^- \rightarrow H_2O + e^- \quad (5)$$

Additionally, because of the catalytic characteristics of NiO, it can dissociate $H_2$ molecules into H atoms ($H_{adsorbed}$), which spill over onto the ZnO surface to react with adsorbed oxygen species ($O^-$) according to following equations [31,32]:

$$H_2 \rightarrow 2H \quad (6)$$

$$2H_{(ads)} + O^- \rightarrow H_2O + e^- \quad (7)$$

As a result of above reactions, the released electrons return to the surface of sensor, which results

Preprints (www.preprints.org) | NOT PEER-REVIEWED | Posted: 20 August 2018 doi:10.20944/preprints201808.0354.v1

in a large decrease in the width of the electron depletion layer on the sensor. Consequently, a response can be observed. Additionally, based on the abundance of ZnO nanograins, there are significant n-ZnO-n-ZnO homojunctions that create potential barriers to the flow of electrons. Modulation of the potential height at homojunctions in the presence of $H_2$ alter the resistance, which eventually contributes to the appearance of a sensor signal. However, it should be noted that because there are very low amounts of NiO in the fabricated sensors, it is unlikely that p-NiO/p-NiO homojunctions significantly affect the final sensing performance of the sensors.

Furthermore, because of the strong reducing effect of hydrogen, the surfaces of the ZnO at the sensing temperature may be partially reduced to metallic Zn. Metallization of the ZnO surface occurs based on the adsorption of $H_2$ atoms on the O sites of the nonpolar surfaces of ZnO. Charge delocalization occurs between Zn and the O−H bonds, and partially occupies the 4s and 3d states of the surface Zn atoms [16]. This surface metallization causes a resistance change in the surfaces of ultrafine ZnO nanograins and contributes to the sensor response (Figure 9a).

Next, we determined why the sensor with the optimized composition (i.e., 0.05 wt% NiO-loaded sensor) showed the highest response to $H_2$ gas. It should be noted that all synthesized NFs were calcined at the same temperature, meaning it is assumed that all sensors have nearly the same morphology, surface area, and grain sizes. Therefore, we excluded these factors in our analysis. This means that the number of p-NiO/n-ZnO heterojunctions and amount of NiO must significantly affect the sensing results. For the 0.97ZnO-0.03NiO composition, the small number of ZnO-NiO heterojunctions will resulted in the weakest sensing performance. In the 0.95ZnO-0.05NiO composition, the response was enhanced by the increased number of ZnO-NiO heterojunctions. Furthermore, this composition had higher amounts of NiO and oxygen ions, which could be easily adsorbed on the surface of the NiO because $Ni^{2+}$ ions are easily oxidized into $Ni^{3+}$ (Figure 9c) [24]. This results in a greater resistance change for the gas sensor [24]. However, for the 0.9ZnO-0.1NiO composition, the response decreased. This is likely a result of the percolation effect, meaning more p-NiO-p-NiO junctions were established in the gas sensor. In fact, instead of being in direct contact with the n-ZnO grains, the p-NiO nanograins established direct contact with each other, resulting in the degradation of sensor sensitivity.

Preprints (www.preprints.org) | NOT PEER-REVIEWED | Posted: 20 August 2018 doi:10.20944/preprints201808.0354.v1

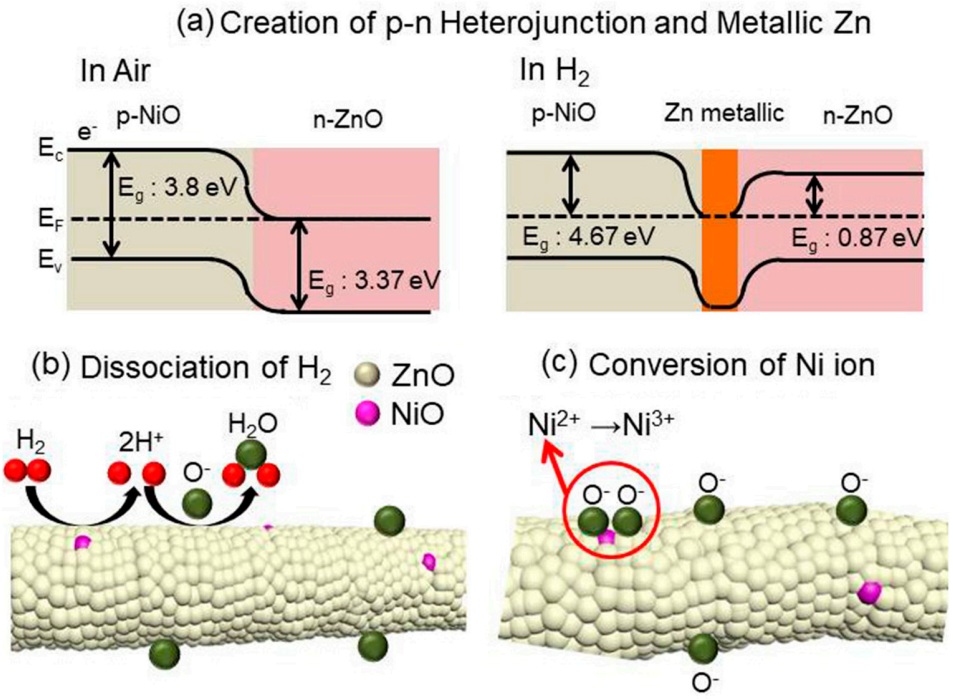


**Figure. 9.** Schematic diagram of sensing mechanism: (a) creation of p-n heterojunctions and metallization of ZnO, (b) dissociation and subsequent oxidation of $H_2$ gas on the surface of gas sensor, and (c) conversion of Ni ions.

## 4. Conclusions

A series of NiO-loaded ZnO NFs were fabricated through the electrospinning technique followed by calcination. Characterization results verified the formation of NiO-loaded ZnO NFs with the desired morphology and composition. Gas sensing results at the optimal sensing temperature of 200 °C demonstrated that the sensor sensitivity decreased when the amount of NiO was greater than 0.05 wt%, indicated that the amount of NiO must be optimized to achieve superior sensing properties. The excellent sensing performance of the optimized sensor can be attributed to the formation of p-n heterojunctions, metallization of ZnO by $H_2$, and catalytic effect of NiO on $H_2$ gas. This study demonstrates the necessity for optimization of p-type loading on n-type NFs to obtain superioer sensing properties.

 doi:10.20944/preprints201808.0354.v1

**Author Contributions**: Experiment and characterizations, J.H.L, J.Y.K and J.-H.K.; Discuss and analyze, A.M and H.W.K; Modify and check, S.S. K.

## Acknowledgments

This research was supported by the International Research & Development Program of the National Research Foundation of Korea (NRF) funded by the Ministry of Science and ICT of Korea (NRF-2017K1A3A1A49070046).

## Conflicts of Interest

The authors declare no conflict of interest.

 doi:10.20944/preprints201808.0354.v1

## References


1. Zhao, M.; Wong, M.H.; Man, H.C.; Ong, C.W. Resistive hydrogen sensing response of Pd-decorated ZnO "nanosponge" film. *Sens. Actuators B: Chem.* **2017**, *249*, 624-631.
2. Mirzaei, A.; Janghorban, K.; Hashemi, B.; Neri, G. Metal-core@metal oxide-shell nanomaterials for gas-sensing applications: A review. *J. Nanopart. Res.* **2015**, *17*, 371.
3. Choi, S.-W.; Kim, S.S. Room temperature co sensing of selectively grown networked ZnO nanowires by Pd nanodot functionalization. *Sens. Actuators B: Chem.* **2012**, *168*, 8-13.
4. Lee, J.-H.; Katoch, A.; Choi, S.-W.; Kim, J.-H.; Kim, H.W.; Kim, S.S. Extraordinary improvement of gas-sensing performances in $SnO_2$ nanofibers due to creation of local p-n heterojunctions by loading reduced graphene oxide nanosheets. *ACS Appl. Mater. & Interf.* **2015**, *7*, 3101-3109.
5. Kwon, Y.J.; Kang, S.Y.; Mirzaei, A.; Choi, M.S.; Bang, J.H.; Kim, S.S.; Kim, H.W. Enhancement of gas sensing properties by the functionalization of ZnO-branched $SnO_2$ nanowires with $Cr_2O_3$ nanoparticles. *Sens. Actuators B: Chem.* **2017**, *249*, 656-666.
6. Kim, J.-H.; Mirzaei, A.; Kim, H.W.; Kim, S.S. Extremely sensitive and selective sub-ppm co detection by the synergistic effect of au nanoparticles and core-shell nanowires. *Sens. Actuators B: Chem.* **2017**, *249*, 177-188.
7. Kim, J.-H.; Lee, J.-H.; Mirzaei, A.; Kim, H.W.; Kim, S.S. Optimization and gas sensing mechanism of n-$SnO_2$-p-$Co_3O_4$ composite nanofibers. *Sens. Actuators B: Chem.* **2017**, *248*, 500-511.
8. Kim, J.-H.; Zheng, Y.; Mirzaei, A.; Kim, H.W.; Kim, S.S. Synthesis and selective sensing properties of rGO/metal-coloaded $SnO_2$ nanofibers. *J. Elec. Mater.* **2017**, *46*, 3531-3541.
9. Abideen, Z.U.; Kim, J.-H.; Mirzaei, A; Kim, H. W; Kim S.S, Sening behavior to ppm-level gases and synergistic sensing mechanism in metal-functionalized rGO-loaded ZnO nanofibers. *Sens. Actuators B: Chem.* **2018**, 252, 1884-1896.
10. Katoch, A.; Kim, J.-H.; Kwon, Y.J.; Kim, H.W.; Kim, S.S. Excellent gas detection of zno nanofibers by loading with reduced graphene oxide nanosheets. *Sens. Actuators B: Chem.* **2015**, *221*, 1499-1507.
11. Wei, W.; Guo, S.; Chen, C.; Sun, L.; Chen, Y.; Guo, W.; Ruan, S. High sensitive and fast formaldehyde gas sensor based on Ag-doped $Fe_2O_3$ nanofibers. *J. Alloy. Comp.* **2017**, *695*, 1122-1127.
12. Woo, J.-A.; Phan, D.-T.; Jung, Y.W.; Jeon, K.-J. Fast response of hydrogen sensor using palladium nanocube-$TiO_2$ nanofiber composites. *Interl. J. Hydrogen Energy* **2017**, *42*, 18754-18761.
13. Mirzaei, A.; Park, S.; Kheel, H.; Sun, G.-J.; Lee, S.; Lee, C. ZnO-capped nanorod gas sensors. *Ceram. Inter.* **2016**, *42*, 6187-6197.
14. Galstyan, V.; Comini, E.; Baratto, C.; Faglia, G.; Sberveglieri, G. Nanostructured ZnO chemical gas sensors. *Ceram. Inter.* **2015**, *41*, 14239-14244.
15. Kim, H.-J.; Lee, J.-H. Highly sensitive and selective gas sensors using p-type oxide semiconductors: Overview. *Sens. Actuators B: Chem.* **2014**, *192*, 607-627.
16. Katoch, A.; Kim, J.-H.; Kwon, Y.J.; Kim, H.W.; Kim, S.S. Bifunctional sensing mechanism of $SnO_2$–ZnO composite nanofibers for drastically enhancing the sensing behavior in $H_2$ gas. *ACS Appl. Mater. & Interf.* **2015**, *7*, 11351-11358.

17. Katoch, A.; Choi, S.-W.; Kim, J.-H.; Lee, J.H.; Lee, J.-S.; Kim, S.S. Importance of the nanograin size on the $H_2S$-sensing properties of ZnO-CuO composite nanofibers. *Sens. Actuators B: Chem.* **2015**, *214*, 111-116.
18. Deng, X.; Zhang, L.; Guo, J.; Chen, Q.; Ma, J. ZnO enhanced NiO-based gas sensors towards ethanol. *Mater. Res. Bull.* **2017**, *90*, 170-174.
19. Gao, H.; Wei, D.; Lin, P.; Liu, C.; Sun, P.; Shimanoe, K.; Yamazoe, N.; Lu, G. The design of excellent xylene gas sensor using Sn-doped nio hierarchical nanostructure. *Sens. Actuators B: Chem.* **2017**, *253*, 1152-1162.
20. Liu, C.; Zhao, L.; Wang, B.; Sun, P.; Wang, Q.; Gao, Y.; Liang, X.; Zhang, T.; Lu, G. Acetone gas sensor based on NiO/ZnO hollow spheres: Fast response and recovery, and low (ppb) detection limit. *J. Colloid Interf. Sci.* **2017**, *495*, 207-215.
21. Kim, J.-H.; Zang Y.; Mirzaei A.; Kim S.S.; Excellent carbon monoxide sensing performance of au-decorated $SnO_2$ nanofibers. *Korean J. Mater. Res.* **2016**, *26*, 741-750.
22. Fan, F.; Zhang, J.; Li, J.; Zhang, N.; Hong, R.; Deng, X.; Tang, P.; Li, D. Hydrogen sensing properties of Pt-Au bimetallic nanoparticles loaded on ZnO nanorods. *Sens. Actuators B: Chem.* **2017**, *241*, 895-903.
23. L.Schlapbach, A.Z. Hydrogen-storage materials for mobile applications. *Nature* **2001**, *414*, 353-358.
24. Liu, C.; Wang, B.; Liu, T.; Sun, P.; Gao, Y.; Liu, F.; Lu, G. Facile synthesis and gas sensing properties of the flower-like nio-decorated ZnO microstructures. *Sens. Actuators B: Chem.* **2016**, *235*, 294-301.
25. Wang, Z.; Li, Z.; Sun, J.; Zhang, H.; Wang, W.; Zheng, W.; Wang, C. Improved hydrogen monitoring properties based on p-NiO/n-$SnO_2$ heterojunction composite nanofibers. *J. of Phys. Chem. C* **2010**, *114*, 6100-6105.
26. Mirzaei, A.; Janghorban, K.; Hashemi, B.; Bonyani, M.; Leonardi, S.G.; Neri, G. A novel gas sensor based on Ag/$Fe_2O_3$ core-shell nanocomposites. *Ceram. Inter.* **2016**, *42*, 18974-18982.
27. Kwon, Y.J.; Mirzaei, A.; Kang, S.Y.; Choi, M.S.; Bang, J.H.; Kim, S.S.; Kim, H.W. Synthesis, characterization and gas sensing properties of ZnO-decorated mwcnts. *Appl. Surf. Sci.***2017**, *413*, 242-252.
28. Mirzaei, A.; Leonardi, S.G.; Neri, G. Detection of hazardous volatile organic compounds (VOCs) by metal oxide nanostructures-based gas sensors: A review. *Ceram. Inter.* **2016**, *42*, 15119-15141.
29. Barsan, N.; Weimar, U. Conduction model of metal oxide gas sensors. *J. Electroceram.* **2001**, *7*, 143-167.
30. Falsafi, F.; Hashemi, B.; Mirzaei, A.; Fazio, E.; Neri, F.; Donato, N.; Leonardi, S.G.; Neri, G. Sm-doped cobalt ferrite nanoparticles: A novel sensing material for conductometric hydrogen leak sensor. *Ceram. Inter.* **2017**, *43*, 1029-1037.
31. Takeguchi, T.; Furukawa, S.-N.; Inoue, M. Hydrogen spillover from nio to the large surface area $CeO_2$–$ZrO_2$ solid solutions and activity of the NiO/$CeO_2$-$ZrO_2$ catalysts for partial oxidation of methane. *J. Catalysis* **2001**, *202*, 14-24.
32. Sanger, A.; Kumar, A.; Kumar, A.; Chandra, R. Highly sensitive and selective hydrogen gas sensor using sputtered grown pd decorated $MnO_2$ nanowalls. *Sens. Actuators B: Chem.* **2016**, *234*, 8-14.

 doi:10.20944/preprints201808.0354.v1

**Figure Captions**

**Figure. 1.** Schematic illustration of preparation steps for the synthesis of NiO-loaded ZnO NFs: (a) preparation of viscous solution for electrospinning, (b) electrospinning procedure, (c) calcination of synthesized NFs, and (d) sensor fabrication.

**Figure. 2.** FE-SEM images: (a) 0.03 wt% NiO-loaded ZnO NFs before calcination, (b) 0.03 wt% NiO-loaded ZnO NFs after calcination, (c) 0.05 wt% NiO-loaded ZnO NFs after calcination, and (d) 0.1 wt% NiO-loaded ZnO NFs after calcination. Insets show corresponding magnified FE-SEM images.

**Figure. 3.** (a) Typical high-magnification TEM image of ZnO-NiO composite NFs, (b) corresponding lattice-resolved TEM image showing the lattice fringes of ZnO and NiO, and (c)-(e) EDS color-mapping analyses of 0.05 wt% NiO-loaded ZnO NFs.

**Figure. 4.** Dynamic normalized resistance curves of 0.05 wt% NiO-loaded ZnO NF sensor for 1-, 5-, and 10-ppm $H_2$ gas at different sensing temperatures.

**Figure. 5.** Dependence of $H_2$ gas response on sensing temperature for 0.05 wt% NiO-loaded ZnO NF sensor.

**Figure. 6.** (a) Response and recovery times of 0.05 wt% NiO-loaded ZnO NF sensor and (b) initial resistance of 0.05 wt% NiO-loaded ZnO NF sensor as a function of sensing temperature.

**Figure. 7.** (a) Dynamic normalized resistance curves of different sensors for various concentrations of $H_2$ gas at optimal sensing temperature of 200 °C and (b) corresponding responses for different sensor compositions.

**Figure. 8.** (a). Dynamic normalized resistance curves of 0.05 wt% NiO-loaded ZnO NF gas sensor for 1-, 5-, and 10-ppm concentrations of $H_2$, CO, and $C_6H_6$ gases at 200 °C. (b) Corresponding selectivity histogram.

**Figure. 9.** Schematic diagram of sensing mechanism: (a) creation of p-n heterojunctions and metallization of ZnO, (b) dissociation and subsequent oxidation of $H_2$ gas on the surface of gas sensor, and (c) conversion of Ni ions.